Study of $N(1440)$ structure via $\gamma^* p \to N(1440)$ transition

A. Kaewsnod,[1,*] K. Xu,[1] Z. Zhao,[1] X. Y. Liu,[1,2] S. Srisuphaphon,[3] A. Limphirat,[1] and Y. Yan[1,†]

[1]*School of Physics and Center of Excellence in High Energy Physics and Astrophysics, Suranaree University of Technology, Nakhon Ratchasima 30000, Thailand*

[2]*School of Physics, Liaoning University, Shenyang 110036, China*

[3]*Department of Physics, Faculty of Science, Burapha University, Chonburi 20131, Thailand*

(Received 21 July 2021; accepted 23 December 2021; published 7 January 2022)

We study the $\gamma^* p \to N^*$ transition of the $N(1440)$ resonance in quark models to reveal the inner structure of the resonance. The $N(1440)$ is assumed in the study: (a) the first radial excitation of the nucleon, where the quark distribution is imported from low-lying baryon mass spectrum calculations, (b) a general radial excitation of the nucleon, and (c) a q^3 state with positive parity. The comparison between the theoretical results and experimental data on the helicity amplitudes $A_{1/2}$ and $S_{1/2}$ and the analysis of the spatial wave function of the $N(1440)$ resonance reveal that the $N(1440)$ resonance is mainly the q^3 first radial excitation.

DOI: 10.1103/PhysRevD.105.016008

I. INTRODUCTION

In recent years, the experiments on electro- and photoproductions of particles have accumulated a large amount of data of helicity amplitudes over the four-momentum transfer Q^2 of virtual photons [1–4]. The most complete experimental data has been obtained for the Roper resonance, $N(1440)$, up to 4.5 GeV^2 [5,6]. Theoretical studies have been carried out to reveal the properties and structures of nucleon resonance states by analyzing the transverse transition amplitudes $A_{1/2}$ and $A_{3/2}$ and longitudinal transition amplitude $S_{1/2}$ over Q^2 in a large range [7–16]. However, the electro- and photoproduction data of the Roper resonance have not been well described by the conventional quark models [7–11] as well as other approaches. The nature of the Roper resonance is still an open question, which is also implied by its large decay width [17] as well as the mass ordering with the lowest negative-parity baryon resonance states $N(1520)$ and $N(1535)$ [18]. Detailed discussion about the Roper resonance may be found in a good review paper [12]. Among a large number of theoretical works, the light-front relativistic quark model [7–9] and the covariant spectator quark model [10], assuming that the $N(1440)$ is the first radial excitation of the q^3 ground state, can give the right sign of the transverse $\gamma^* p \to N(1440)$ amplitudes and reproduce the experimental data of the transverse amplitudes at high Q^2, but fail to describe the data of the $N(1440)$ helicity amplitude at low Q^2. Mass spectrum calculations [19,20], where the mass ordering problem of $N(1440)$, $N(1520)$, and $N(1535)$ is tackled by including ground state light pentaquark components in the negative-parity nucleon resonances, point out that the $N(1440)$ might be mainly the first radial excitation of the nucleon.

In this work we study the helicity transition amplitudes of the $N(1440)$ resonance in the process $p\gamma^* \to N^*$ to reveal the inner structure of the resonance. The impulse approximation is applied in the work, where the electromagnetic current is induced by free single quark currents. The paper is organized as follows. In Sec. II, we study the proton electric form factor to justify the impulse approximation and the dominance of three-quark core. In Sec. III, the $A_{1/2}$ and $S_{1/2}$ of the $N(1440)$ resonance are investigated in three cases, namely, the spatial wave function of the $N(1440)$ imported from a mass spectrum study as the first radial excitation of the nucleon, the $N(1440)$ is a general radial excitation of the nucleon, and the $N(1440)$ is just a q^3 state with positive parity. The quark distribution of the $N(1440)$ is extracted in Sec. IV from the results in Sec. III. A summary is given in Sec. V.

II. PROTON FORM FACTOR OF THREE-QUARK CORE

In this section we evaluate the proton electric form factor in the lowest order approximation, where the proton takes the three-quark ground state and the electromagnetic current is induced by the free single quark current (impulse

*a.kaewsnod@gmail.com
†yupeng@g.sut.ac.th

Published by the American Physical Society under the terms of the Creative Commons Attribution 4.0 International license. Further distribution of this work must maintain attribution to the author(s) and the published article's title, journal citation, and DOI. Funded by SCOAP³.

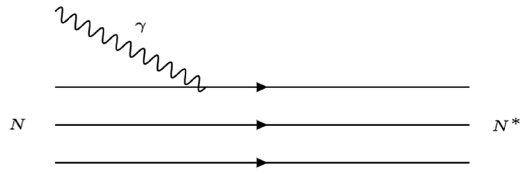

FIG. 1. Diagram of $N\gamma^* \to N^*$ transition where both the initial nucleon (N) and final nucleon resonance (N^*) are in the three-quark picture.

approximation) as shown in Fig. 1. The purpose of the study is to see if the impulse approximation is reasonable for the present study and if the proton electric form factor is dominated by the three-quark core. We first evaluate the proton electric form factor in the impulse approximation of the electromagnetic current, with the proton wave function imported from the study of low-lying baryon mass spectra [20]. Then we fit the experimental data of the proton electric form factor, assuming that the proton is the ground state of three quarks, to extract the proton wave function.

Studies of the transition form factors of the $N(1440)$ in the light-front quark model [21–23], where the single quark current operator is assumed to provide the main mechanism for the electromagnetic excitation of the nucleon and the two-body exchange currents are neglected, lead to a realistic description of the form factors and helicity amplitudes. As discussed in Ref. [24], however, two-body currents may affect the $A_{1/2}$ and $S_{1/2}$ helicity amplitudes of the $\gamma^* p \to N^*$ process. Details concerning the gluon exchange current may be found in Refs. [25,26].

The proton electric form factor G_E, the time component of the electromagnetic current, is derived in the Breit frame. The momenta of the initial-state nucleon, final-state nucleon, and photon are respectively defined as $P_i = (E_N, 0, 0, -|\boldsymbol{k}/2|)$, $P_f = (E_N, 0, 0, |\boldsymbol{k}/2|)$, $k = (0, 0, 0, |\boldsymbol{k}|)$ in the Breit frame, with E_N and $\boldsymbol{k}$ being the energy and three-momentum of the photon. The photon energy is $\omega = 0$ as $\boldsymbol{P}_i + \boldsymbol{P}_f = 0$ in the Breit frame. In the impulse approximation in Fig. 1, the transition $p\gamma^* \to p$ take the form,

$$G_E = \left\langle N, S_z' = \frac{1}{2}\middle| q_1' q_2' q_3' \right\rangle T_B(q_1 q_2 q_3 \to q_1' q_2' q_3') \times \left\langle q_1 q_2 q_3 \middle| N, S_z = \frac{1}{2} \right\rangle \Big|_{\text{Breit frame}}, \quad (1)$$

where $\langle q_1 q_2 q_3 | N, S_z \rangle$ are the N wave functions in the three-quark picture. The matrix elements of electromagnetic transition in the Breit frame are represented as

$$T_B(q_1 q_2 q_3 \to q_1' q_2' q_3') = e_3 \bar{u}_{s'}(p') \gamma^\mu u_s(p) \epsilon_\mu(k) \langle q_1' q_2' | q_1 q_2 \rangle = e_3 T^B_{s's} \langle q_1' q_2' | q_1 q_2 \rangle, \quad (2)$$

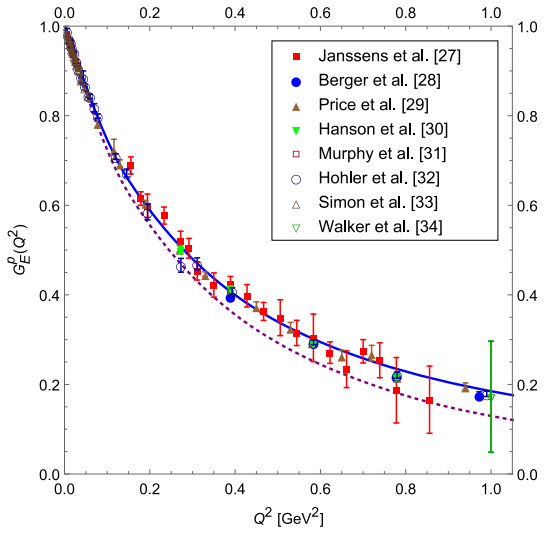

FIG. 2. Proton electric form factor G_E compared to experimental data. The solid curve is the fitting result that leads to the proton spatial wave function to be used in the helicity amplitude calculations, and the short dashed curve is derived with the proton spatial wave function from low-lying baryon mass spectrum calculations. The experimental data are taken from [27–34].

where e_3 and $u_{s(s')}$ are the electric charge and the Dirac spinners of the third quark with s', s being the single quark spin projections (spin up $\uparrow$ and spin down $\downarrow$), and λ is the helicity of the photon. In the work, the mass of u and d quarks are taken to be $m = 5$ MeV. The polarization vector of the photon in Eq. (2) is defined as $\epsilon_\mu = (1, 0, 0, 0)$. The matrix elements $T^B_{s's}$ are shown in Appendix A.

The calculated proton electric form factor G_E, with the proton spatial wave function imported from the mass spectra study in the three quark picture, is shown as the dotted curve in Fig. 2. It is found in Fig. 2 that the theoretical results for the proton electric form factor G_E are consistent with the experimental data. It is a surprise that the proton wave function derived from the baryon mass spectrum calculation leads to good results for the electric form factor at lower Q^2, which may imply that the three-quark core dominantly contribute to the proton electric form factor. One may believe that meson cloud contributions may account for a considerable part of the proton electric form factor at lower Q^2. However, this work reveals that the three-quark core dominantly contribute to the proton electric form factor, even for very low Q^2, and meson cloud contributions may be negligible for the proton electric form factor.

We fit the experimental data of the proton form factor, assuming that the proton is a three-quark ground state. The fitted results are shown as the solid curve in Fig. 2. The proton spatial wave function extracted from the theoretical result of the proton electric form factor in Fig. 2 will be employed to study the $N(1440)$ in the next section.

III. HELICITY AMPLITUDES WITH $N(1440)$ AS THREE QUARK STATES

We study the $N\gamma^* \to N^*$ electromagnetic transition in the constituent quark model in the impulse approximation as shown in Fig. 1. The transverse helicity amplitude $A_{1/2}$ and the longitudinal helicity amplitude $S_{1/2}$ are usually defined in the N^* rest frame. The momentum of the nucleon P_i, the momentum of the resonance state P_f, and the photon momentum $k = P_f - P_i$ are defined as $P_i = (E_N, 0, 0, -|\boldsymbol{k}|)$, $P_f = (M_{N^*}, 0, 0, 0)$, $k = (\omega, 0, 0, |\boldsymbol{k}|)$. The square of the four-momentum transfer is expressed by $Q^2 = -k^2 = |\boldsymbol{k}|^2$. One has

$$\begin{aligned} E_N &= \frac{M_{N^*}^2 + M_N^2 + Q^2}{2M_{N^*}}, \\ \omega &= \frac{M_{N^*}^2 - M_N^2 - Q^2}{2M_{N^*}}, \\ |\boldsymbol{k}| &= \left[Q^2 + \left(\frac{M_{N^*}^2 - M_N^2 - Q^2}{2M_{N^*}}\right)^2\right]^{\frac{1}{2}}. \end{aligned} \tag{3}$$

The transverse and longitudinal helicity amplitudes of electromagnetic transitions of the $\gamma^* p \to N^*$ take the form,

$$\begin{aligned} A_{1/2} &= \frac{1}{\sqrt{2K}} \left\langle N^*, S_z' = \frac{1}{2} \middle| q_1' q_2' q_3' \right\rangle \\ &\quad \times T(q_1 q_2 q_3 \to q_1' q_2' q_3') \left\langle q_1 q_2 q_3 \middle| N, S_z = -\frac{1}{2} \right\rangle, \\ S_{1/2} &= \frac{1}{\sqrt{2K}} \frac{|\boldsymbol{k}|}{Q} \left\langle N^*, S_z' = \frac{1}{2} \middle| q_1' q_2' q_3' \right\rangle \\ &\quad \times T(q_1 q_2 q_3 \to q_1' q_2' q_3') \left\langle q_1 q_2 q_3 \middle| N, S_z = \frac{1}{2} \right\rangle, \end{aligned} \tag{4}$$

with

$$K = \frac{M_{N^*}^2 - M_N^2}{2M_{N^*}}, \tag{5}$$

where K is the real-photon momentum in the N^* rest frame, M_{N^*} and M_N are respectively the N^* and N masses, and $\langle q_1 q_2 q_3 | N, S_z \rangle$ and $\langle q_1' q_2' q_3' | N^*, S_z' \rangle$ are the N and N^* wave functions in the three-quark picture. $T(q_1 q_2 q_3 \to q_1' q_2' q_3')$ in Eq. (4) is the transition amplitude of the process $\gamma q \to q'$ displayed in Fig. 1, which can be calculated in the standard language of quantum field theory,

$$\begin{aligned} T(q_1 q_2 q_3 \to q_1' q_2' q_3') &= e_3 \bar{u}_{s'}(p') \gamma^\mu u_s(p) \epsilon_\mu^\lambda(k) \langle q_1' q_2' | q_1 q_2 \rangle \\ &= e_3 T_{s's}^\lambda \langle q_1' q_2' | q_1 q_2 \rangle, \end{aligned} \tag{6}$$

where e_3 and $u_{s(s')}$ are the electric charge and the Dirac spinners of the third quark with s', s being the single quark spin projections (spin up $\uparrow$ and spin down $\downarrow$), and λ is the helicity of the photon. The photon polarization vectors $\epsilon_\mu^\lambda(k)$ of the longitudinal ($\lambda = 0$) and transverse ($\lambda = 1$) helicity amplitudes in the Lorentz gauge are defined as $\epsilon_\mu^0 = \frac{1}{Q}(|\boldsymbol{k}|, 0, 0, \omega)$ and $\epsilon_\mu^+ = -\frac{1}{\sqrt{2}}(0, 1, i, 0)$. The matrix elements $T_{s's}^\lambda$ are shown in Appendix B. In Eq. (4), one sums over all possible quantum states of the intermediate three quarks and integrates over the momenta of all quarks.

In this section, the helicity amplitudes $A_{1/2}$ and $S_{1/2}$ of the $N(1440)$ resonance will be evaluated with different $N(1440)$ wave functions, assuming that the $N(1440)$ is in the three-quark configuration, but may contain higher radial excitations of the nucleon or may be just a positive parity state. We do three calculations:

A: The spatial wave functions of the proton and the Roper resonance are derived in the study of low-lying baryon mass spectra [20], where the proton is assumed to be the three-quark ground state and the $N(1440)$ to be the first radial excitation of the nucleon.

B (Fitting I): The proton and the $N(1440)$ spatial wave functions are orthogonal each other, $\langle \psi_p^O | \psi_{N(1440)}^O \rangle = 0$ which constrains the $N(1440)$ spatial wave function to be the radial excitations of the nucleon. In this calculation we employ the proton spatial wave function extracted from the theoretical result (solid curve) of the proton electric form factor in Fig. 2. The fitting is expected to reveal if the $N(1440)$ may consist of higher excitations of the nucleon.

C (Fitting II): The proton and the $N(1440)$ spatial wave functions may not be orthogonal each other, which allows the $N(1440)$ spatial wave function consist of other components beside radial excitations of the nucleon. The proton spatial wave function is same as the one in Fitting I. The purpose of the fitting is to see how much other components rather than radial excitations of the nucleon the $N(1440)$ may consist of.

The theoretical results of the helicity amplitudes of the $N(1440)$ resonance are shown in Figs. 3 and 4 with the dotted lines for Calculation A, the dash-dotted lines for Calculation B (Fitting I), and the solid lines for Calculation C (Fitting II). For both the $A_{1/2}$ and $S_{1/2}$, the theoretical results in Calculation A can fairly describe the experimental data at large Q^2 region ($1.5 \le Q^2 \le 4.5$ GeV^2). This is consistent with the theoretical results in the light-front relativistic quark model [7] and covariant spectator quark model [10]. The theoretical results of the helicity amplitude $A_{1/2}$ are in the right tendency of the $A_{1/2}$ data and can give the right sign at the real photon point though the discrepancy between the theoretical results and the experimental data is obvious. Considering that the $N(1440)$ wave

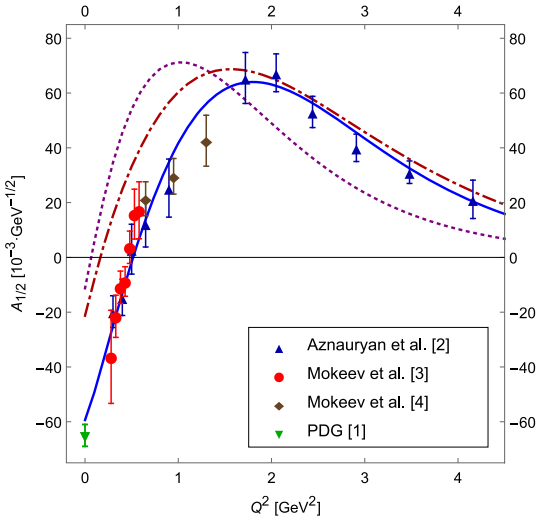

FIG. 3. Transverse helicity amplitude $A_{1/2}$ of the $p\gamma^* \to N(1440)$ transition compared to the measurements. The short dashed, dash-dotted, and solid curves are the results with the $N(1440)$ spatial wave function from the low-lying baryon mass spectrum calculations, in Fitting I, and in Fitting II, respectively. The experimental data are taken from [1–4].

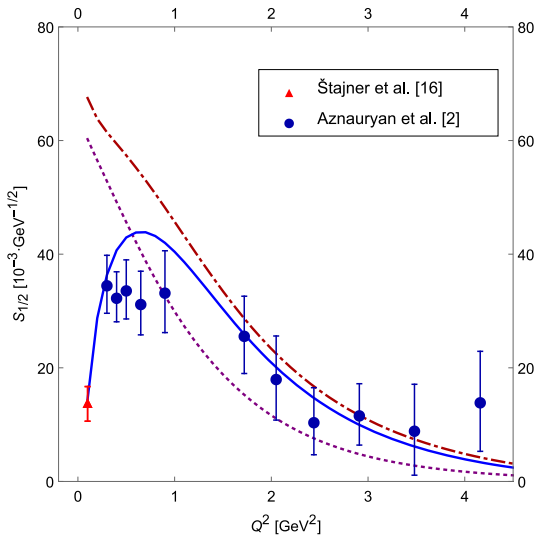

FIG. 4. Longitudinal helicity amplitude $S_{1/2}$ of $p\gamma^* \to N(1440)$ transition in comparison with experimental data [2,16]. The short dashed, dash-dotted, and solid curves are the results with the $N(1440)$ spatial wave function from the low-lying baryon mass spectrum calculations, in Fitting I, and in Fitting II, respectively.

function employed in the calculation is imported, without any modification, from the baryon mass spectrum calculation, one may have a good belief that the $N(1440)$ is mainly a three-quark state, the first radial excitation of the proton. The theoretical results of the $S_{1/2}$ in Calculation A at low Q^2 region are largely inconsistent with the experimental data, giving a much bigger value at the real photon point, which may indicate that the $N(1440)$ might have some other components rather than the first radial excitation of the nucleon in the three quark picture.

It is found in Figs. 3 and 4 that the theoretical results of the helicity amplitude $A_{1/2}$ in Fitting I improve more or less the results in Calculation A, especially for small Q^2, but for the amplitude $S_{1/2}$ the results here are rather similar to the ones in Calculation A without any improvement. Therefore, one may conclude that the results in Fitting I rule out that the $N(1440)$ may be composed of a sizeable component of higher radial excitations of the nucleon. The failure of the present model calculations A and B in describing the low momentum behavior of $S_{1/2}$ implies that the single quark transition models and/or the three-quark picture of baryons may miss important degrees of freedom, such as quark-antiquark pair components in the $N(1440)$ wave function and two-body electromagnetic current operators. It is revealed that the contributions from quark-antiquark pair currents (meson cloud) is dominant in the neutron charge form factor [35,36] and also important in the $\gamma N \to \Delta(1232)$ and $\gamma N \to N(1440)$ transition form factors [24,37] at low Q^2. The results in Fig. 8 in Ref. [24], giving the right sign and magnitude at the photon point, may tell that exchange currents have a large effect on $S_{1/2}$. As mentioned in Ref. [24], however, that the two-body current contributions to the $A_{1/2}$ helicity amplitude of the $\gamma p \to N(1440)$ process at low Q^2 might be overestimated so that the theoretical results are not well consistent with the recent experimental data.

As shown in Figs. 3 and 4, the Fitting II results are in a perfect fit to the amplitude $A_{1/2}$ and a very reasonable fit to the amplitude $S_{1/2}$, particularly to the two values at the real photon point. The results imply that the $N(1440)$ may consist of components other than radial excitations of three quarks. The larger tail of the $N(1440)$ radial wave function extracted from Fitting II, as shown in Fig. 5, may indicate that the quark-antiquark pair components (meson cloud, baryon-meson molecule and pentaquark) in the $N(1440)$ wave function may play important roles. Systematic studies are necessary, including these components into the $N(1440)$ and also contributions of two-body currents.

IV. EXTRACTION OF QUARK DISTRIBUTION OF $N(1440)$

To see the inner structure of the $N(1440)$ closely, we extract the spatial wave functions from the calculations in Secs. II and III. Shown in Fig. 5 are the $N(1440)$ spatial wave functions with respect to the relative distance between the quark to the center of mass, where the solid and dashed

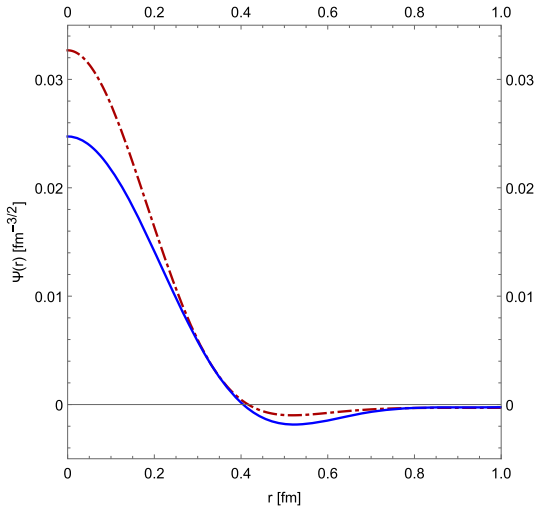

FIG. 5. $N(1440)$ spatial wave functions with respect to the relative distance between the quark to the center of mass: dash-dotted curve from Fitting I and solid curve from Fitting II.

curves are for the $N(1440)$ in Fitting I and Fitting II, respectively. Considering the full permutation symmetry of the three-quark baryon state, we set $|\boldsymbol{r}_\lambda| = |\boldsymbol{r}_\rho|$, where $\boldsymbol{r}_\rho = \frac{1}{\sqrt{2}}(\boldsymbol{r}_1 - \boldsymbol{r}_2)$ and $\boldsymbol{r}_\lambda = \frac{1}{\sqrt{6}}(\boldsymbol{r}_1 + \boldsymbol{r}_2 - 2\boldsymbol{r}_3)$ to project the three-dimensional spatial wave functions to a 2D plot. The nonorthogonality between the proton spatial wave function and the $N(1440)$ one derived in Fitting II is $|\langle\psi_p^O|\psi_{N(1440)}^O\rangle|^2 = 0.03$, indicting that the $N(1440)$ may be composed of components rather than the radial excitations of three quarks.

Figure 5 shows that the quark distribution about the center of mass from Fitting II is lower than the one from Fitting I, and the tail of the $N(1440)$ spatial wave function from Fitting II is larger after the node. The results may indicate that the quark-antiquark pair components (meson cloud, baryon-meson molecule and pentaquark) in the $N(1440)$ wave function may play important roles.

V. SUMMARY

In this work, we have studied the proton electric form factor and the helicity amplitudes of the $N(1440)$ resonance via the process $p\gamma^* \to N^*$. The spatial wave functions of the proton and $N(1440)$ are extracted by fitting the theoretical results to the experimental data of the proton electric form factor and helicity amplitudes.

It is found that the proton wave function derived in the baryon mass spectrum study in the three-quark picture leads to an almost perfect proton electric form factor, particularly at low Q^2. One may conclude that the meson cloud contribution to the proton electric form factor is negligible.

The work supports the argument that the $N(1440)$ resonance is mainly the first radial excited state of the nucleon. However, the Roper may be composed of small components rather than radial excitations of three quarks, such as D-wave three quark states, hadronic molecule states, and pentaquarks. Further studies including these components into the $N(1440)$ and also contributions of two-body currents are under way.

ACKNOWLEDGMENTS

This work was supported by (i) Suranaree University of Technology (SUT), (ii) Thailand Science Research and Innovation (TSRI), and (iii) National Science Research and Innovation Fund (NSRF), Project No. 160355. A. K. and Y. Y. acknowledge support from TSRI-Royal Golden Jubilee Ph.D. (RGJ-PHD) Program (Grant No. PHD/0242/2558) and SUT-OROG scholarship (Contract No. 46/2558).

APPENDIX A: MATRIX ELEMENTS OF $\gamma q \to q'$ FOR PROTON ELECTRIC FORM FACTOR

The matrix elements of the single quark transition $\gamma q \to q'$ for the proton electric form factor are derived in detail,

$$
\begin{aligned}
T^B_{\uparrow\uparrow} &= \left[\frac{(E'+m)(E+m)}{4E'E}\right]^{\frac{1}{2}}\left(1 + \frac{p'_z p_z + 2p'_- p_+}{(E'+m)(E+m)}\right),\\
T^B_{\uparrow\downarrow} &= \left[\frac{(E'+m)(E+m)}{4E'E}\right]^{\frac{1}{2}}\left(\frac{\sqrt{2}(p'_z p_- - p'_- p_z)}{(E'+m)(E+m)}\right),\\
T^B_{\downarrow\uparrow} &= \left[\frac{(E'+m)(E+m)}{4E'E}\right]^{\frac{1}{2}}\left(\frac{\sqrt{2}(-p'_z p_+ + p'_+ p_z)}{(E'+m)(E+m)}\right),\\
T^B_{\downarrow\downarrow} &= \left[\frac{(E'+m)(E+m)}{4E'E}\right]^{\frac{1}{2}}\left(1 + \frac{p'_z p_z + 2p'_+ p_-}{(E'+m)(E+m)}\right),
\end{aligned}
\tag{A1}
$$

where E and E' respectively are the energies of the initial and final interacting quarks with the dynamical quark mass of u and d quarks as m. The momentum $p_\pm$ are defined by $p_\pm = \frac{1}{\sqrt{2}}(p_x \pm i p_y)$.

APPENDIX B: MATRIX ELEMENTS OF $\gamma q \to q'$ FOR HELICITY AMPLITUDES

The matrix elements of the single quark transition $\gamma q \to q'$ for the helicity $\lambda = 0, 1$ are derived in detail,

$$
\begin{aligned}
T^0_{\uparrow\uparrow} &= \left[\frac{(E'+m)(E+m)}{4E'E}\right]^{\frac{1}{2}}\left[\frac{|\boldsymbol{k}|}{Q}\left(1+\frac{p'_z p_z + 2p'_- p_+}{(E'+m)(E+m)}\right) \quad -\frac{\omega}{Q}\left(\frac{p_z}{E+m}+\frac{p'_z}{E'+m}\right)\right],\\
T^0_{\uparrow\downarrow} &= \left[\frac{(E'+m)(E+m)}{4E'E}\right]^{\frac{1}{2}}\left[\frac{|\boldsymbol{k}|}{Q}\left(\frac{\sqrt{2}(p'_z p_- - p'_- p_z)}{(E'+m)(E+m)}\right) \quad -\frac{\omega}{Q}\left(\frac{\sqrt{2}p_-}{E+m}-\frac{\sqrt{2}p'_-}{E'+m}\right)\right],\\
T^0_{\downarrow\uparrow} &= \left[\frac{(E'+m)(E+m)}{4E'E}\right]^{\frac{1}{2}}\left[\frac{|\boldsymbol{k}|}{Q}\left(\frac{\sqrt{2}(-p'_z p_+ + p'_+ p_z)}{(E'+m)(E+m)}\right) \quad -\frac{\omega}{Q}\left(\frac{-\sqrt{2}p_+}{E+m}+\frac{\sqrt{2}p'_+}{E'+m})\right)\right],\\
T^0_{\downarrow\downarrow} &= \left[\frac{(E'+m)(E+m)}{4E'E}\right]^{\frac{1}{2}}\left[\frac{|\boldsymbol{k}|}{Q}\left(1+\frac{p'_z p_z + 2p'_+ p_-}{(E'+m)(E+m)}\right) \quad -\frac{\omega}{Q}\left(\frac{p_z}{E+m}+\frac{p'_z}{E'+m}\right)\right],\\
T^+_{\uparrow\uparrow} &= \left[\frac{(E'+m)(E+m)}{4E'E}\right]^{\frac{1}{2}}\left[\frac{2p_+}{E+m}\right],\\
T^+_{\uparrow\downarrow} &= \left[\frac{(E'+m)(E+m)}{4E'E}\right]^{\frac{1}{2}}\left[-\frac{\sqrt{2}p_z}{E+m}+\frac{\sqrt{2}p'_z}{E'+m}\right],\\
T^+_{\downarrow\uparrow} &= 0,\\
T^+_{\downarrow\downarrow} &= \left[\frac{(E'+m)(E+m)}{4E'E}\right]^{\frac{1}{2}}\left[\frac{2p'_+}{E'+m}\right],
\end{aligned}
\tag{B1}
$$

where E and E' are respectively the energies of the initial and final interacting quarks with the dynamical quark mass of u and d quarks as m, and $p_\pm = \frac{1}{\sqrt{2}}(p_x \pm i p_y)$.

[1] P. A. Zyla *et al.*, Review of particle physics, Prog. Thoer. Exp. Phys. **2020**, 083C01 (2020).

[2] I. G. Aznauryan, V. D. Burkert, A. S. Biselli, H. Egiyan, K. Joo, W. Kim, K. Park, L. C. Smith, M. Ungaro, K. P. Adhikari, M. Anghinolfi, H. Avakian, J. Ball, M. Battaglieri, V. Batourine *et al.*, Electroexcitation of nucleon resonances from CLAS data on single pion electroproduction, Phys. Rev. C **80**, 055203 (2009).

[3] V. I. Mokeev, V. D. Burkert, L. Elouadrhiri, G. V. Fedotov, E. N. Golovatch, R. W. Gothe, B. S. Ishkhanov, E. L. Isupov, K. P. Adhikari, M. Aghasyan, M. Anghinolfi, H. Avakian, H. Baghdasaryan, J. Ball, N. A. Baltzell *et al.*, Experimental study of the $P_{11}(1440)$ and $D_{13}(1520)$ resonances from the CLAS data on $ep \to e'\pi^+\pi^- p'$, Phys. Rev. C **86**, 035203 (2012).

[4] V. I. Mokeev, V. D. Burkert, D. S. Carman, L. Elouadrhiri, G. V. Fedotov, E. N. Golovatch, R. W. Gothe, K. Hicks, B. S. Ishkhanov, E. L. Isupov, and Iu. Skorodumina, New results from the studies of the $n(1440)1/2^+$, $n(1520)3/2^-$, and $\Delta(1620)1/2^-$ resonances in exclusive $ep \to e'p'\pi^+\pi^-$ electroproduction with the CLAS detector, Phys. Rev. C **93**, 025206 (2016).

[5] L. Tiator, D. Drechsel, S. S. Kamalov, and M. Vanderhaeghen, Electromagnetic excitation of nucleon resonances, Eur. Phys. J. Special Topics **198**, 141 (2011).

[6] L. Tiator, D. Drechsel, S. S. Kamalov, and M. Vanderhaeghen, Baryon resonance analysis from MAID, Chin. Phys. C **33**, 1069 (2009).

[7] I. G. Aznauryan, Electroexcitation of the Roper resonance in relativistic quark models, Phys. Rev. C **76**, 025212 (2007).

[8] I. G. Aznauryan, V. D. Burkert, W. Kim, K. Park, G. Adams, M. J. Amaryan, P. Ambrozewicz, M. Anghinolfi, G. Asryan, H. Avakian, H. Bagdasaryan, N. Baillie, J. P. Ball, N. A. Baltzell, S. Barrow *et al.*, Electroexcitation of the Roper resonance for $1.7 < Q^2 < 4.5$ GeV^2 in $ep \to en\pi^+$, Phys. Rev. C **78**, 045209 (2008).

[9] S. Capstick, B. D. Keister, and D. Morel, Nucleon to resonance form factor calculations, J. Phys. Conf. Ser. **69**, 012016 (2007).

[10] G. Ramalho and K. Tsushima, Valence quark contributions for the $\gamma n \to P_{11}(1440)$ form factors, Phys. Rev. D **81**, 074020 (2010).

[11] B. Golli, S. Sirca, and M. Fiolhais, Pion electro-production in the Roper region in chiral quark models, Eur. Phys. J. A **42**, 185 (2009).

[12] V. D. Burkert and C. D. Roberts, Colloquium: Roper resonance: Toward a solution to the fifty year puzzle, Rev. Mod. Phys. **91**, 011003 (2019).

[13] Q. B. Li and D. O. Riska, Role of $q\bar{q}$ components in the $n(1440)$ resonance, Phys. Rev. C **74**, 015202 (2006).

[14] I. T. Obukhovsky, A. Faessler, D. K. Fedorov, T. Gutsche, and V. E. Lyubovitskij, Electroproduction of the Roper resonance on the proton: The role of the three-quark core and the molecular $n\sigma$ component, Phys. Rev. D **84**, 014004 (2011).

[15] F. Cano and P. Gonzalez, A consistent explanation of the Roper phenomenology, Phys. Lett. B **431**, 270 (1998).

[16] S. Štajner, P. Achenbach, T. Beranek, J. Beričič, J. C. Bernauer, D. Bosnar, R. Böhm, L. Correa, A. Denig, M. O. Distler, A. Esser, H. Fonvieille, J. M. Friedrich, I. Friščič, S. Kegel, Y. Kohl, H. Merkel *et al.*, Beam-Recoil Polarization Measurement of π^0 Electroproduction on the Proton in the Region of the Roper Resonance, Phys. Rev. Lett. **119**, 022001 (2017).

[17] A. V. Sarantsev *et al.*, New results on the Roper resonance and the P(11) partial wave, Phys. Lett. B **659**, 94 (2008).

[18] S. Capstick and W. Roberts, Quark models of baryon masses and decays, Prog. Part. Nucl. Phys. **45**, S241 (2000).

[19] K. Xu, A. Kaewsnod, X. Y. Liu, S. Srisuphaphon, A. Limphirat, and Y. Yan, Complete basis for the pentaquark wave function in a group theory approach, Phys. Rev. C **100**, 065207 (2019).

[20] K. Xu, A. Kaewsnod, Z. Zhao, X. Y. Liu, S. Srisuphaphon, A. Limphirat, and Y. Yan, Pentaquark components in low-lying baryon resonances, Phys. Rev. D **101**, 076025 (2020).

[21] S. Capstick and B. D. Keister, Baryon current matrix elements in a light front framework, Phys. Rev. D **51**, 3598 (1995).

[22] F. Cardarelli, E. Pace, G. Salm, and S. Simula, Electroproduction of the Roper resonance and the constituent quark model, Phys. Lett. B **397**, 13 (1997), ISSN 0370-2693.

[23] C. S. An and B. S. Zou, The role of the $qqqq\bar{q}$ components in the electromagnetic transition $\gamma^* \mathrm{N} \to \mathrm{N}^*(1535)$, Eur. Phys. J. A **39**, 195 (2009).

[24] U. Meyer, E. Hernández, and A. J. Buchmann, Exchange currents in nucleon electroexcitation, Phys. Rev. C **64**, 035203 (2001).

[25] A. Buchmann, Y. Yamauchi, and A. Faessler, The one-gluon exchange current in the quark cluster model of the deuteron, Phys. Lett. B **225**, 301 (1989), ISSN 0370-2693.

[26] A. Buchmann, Y. Yamauchi, and A. Faessler, The one-gluon exchange current and the electromagnetic properties of the deuteron, Prog. Part. Nucl. Phys. **24**, 333 (1990), ISSN 0146-6410.

[27] T. Janssens, R. Hofstadter, E. B. Hughes, and M. R. Yearian, Proton form factors from elastic electron-proton scattering, Phys. Rev. **142**, 922 (1966).

[28] C Berger, V. Burkert, G. Knop, B. Langenbeck, and K. Rith, Electromagnetic form-factors of the proton at squared four momentum transfers between 10 and 50 fm^{-2}, Phys. Lett. **35B**, 87 (1971).

[29] L. E. Price, J. R. Dunning, M. Goitein, K. Hanson, T. Kirk, and R. Wilson, Backward-angle electron-proton elastic scattering and proton electromagnetic form-factors, Phys. Rev. D **4**, 45 (1971).

[30] K. M. Hanson, J. R. Dunning, M. Goitein, T. Kirk, L. E. Price, and Richard Wilson, Large-angle quasielastic electron-deuteron scattering, Phys. Rev. D **8**, 753 (1973).

[31] J. J. Murphy, Y. M. Shin, and D. M. Skopik, Proton form factor from 0.15 to 0.79 fm^{-2}, Phys. Rev. C **9**, 2125 (1974).

[32] G. Hhler, E. Pietarinen, I. Sabba-Stefanescu, F. Borkowski, G. G. Simon, V. H. Walther, and R. D. Wendling, Analysis of electromagnetic nucleon form factors, Nucl. Phys. **B114**, 505 (1976), ISSN 0550-3213.

[33] G. G. Simon, C. Schmitt, F. Borkowski, and V. H. Walther, Absolute electron proton cross-sections at low momentum transfer measured with a high pressure gas target system, Nucl. Phys. **A333**, 381 (1980).

[34] R. C. Walker, B. W. Filippone, J. Jourdan, R. Milner, R. McKeown, D. Potterveld, L. Andivahis, R. Arnold, D. Benton, P. Bosted, G. deChambrier, A. Lung, S. E. Rock, Z. M. Szalata, A. Para *et al.*, Measurements of the proton elastic form factors for $1 \leq Q^2 \leq 3$ $(\mathrm{GeV}/c)^2$ at SLAC, Phys. Rev. D **49**, 5671 (1994).

[35] A. Buchmann, E. Hernndez, and K. Yazaki, Gluon and pion exchange currents in the nucleon, Phys. Lett. B **269**, 35 (1991), ISSN 0370-2693.

[36] A. Buchmann, E. Hernndez, and K. Yazaki, Gluon, pion and confinement exchange currents in the nucleon, Nucl. Phys. **A569**, 661 (1994), ISSN 0375-9474.

[37] A. J. Buchmann, E. Hernández, and A. Faessler, Electromagnetic properties of the $\Delta(1232)$, Phys. Rev. C **55**, 448 (1997).